Broadband albedo of Arctic sea ice from MERIS optical data

Christine Pohl[1], Larysa Istomina[1], Steffen Tietsche[2], Evelyn Jäkel[3], Johannes Stapf[3], Gunnar Spreen[1],
and Georg Heygster[1]

[1]Institute of Environmental Physics, University of Bremen, Otto-Hahn-Allee 1, 28359 Bremen, Germany
[2]European Centre for Medium-Range Weather Forecasts, Shinfield Park, Reading, RG2 9AX, United Kingdom
[3]Leipzig Institute for Meteorology, University of Leipzig, Stephanstr. 3, 04103 Leipzig, Germany

Correspondence: Christine Pohl (cpohl@iup.physik.uni-bremen.de)

Abstract. Summer in the Arctic is the season when the sea ice covered ocean experiences rapid changes in its sea ice concentration, the surface albedo, and the melt pond fraction. These processes drastically affect the energy balance of the region and it is a challenge for climate models to represent those correctly.

In this paper, the broadband albedo (300 – 3000 nm) of Arctic sea ice is derived from Medium Resolution Imaging Spec-
5   trometer (MERIS) optical swath data by transforming the spectral albedo as an output from the Melt Pond Detector (MPD) algorithm by a newly developed spectral-to-broadband conversion (STBC). The new STBC replaces the previously applied spectral averaging method to provide a more accurate broadband albedo product which approaches the accuracy of 0.02 – 0.05 required in climate simulations and allows a direct comparison to broadband albedo values from climate models.

The STBC is derived empirically from spectral and broadband albedo measurements over landfast ice. It is validated on a
10 variety of simultaneous spectral and broadband field measurements over Arctic sea ice, is compared to existing conversion techniques and shows a better performance than the currently published algorithms. The root mean square deviation (RMSD) between measured and broadband albedo converted by the STBC is 0.02. Other conversion techniques, the spectral averaging method and the linear combination of albedo values from four MERIS channels, achieve higher RMSDs of 0.09 and 0.05. The improved MERIS derived broadband albedo values are validated with airborne measurements. Results show a smaller RMSD
15 of 0.04 for landfast ice than the RMSD of 0.07 for drifting ice.

The MERIS derived broadband albedo is compared to broadband albedo from ERA5 reanalysis to examine the albedo parameterization used in ERA5. Both albedo products agree in the large-scale pattern. However, consistency in point-to-point comparison is rather poor, with correlations between 0.71 and 0.76 and RMSD in excess of 0.12. This suggests that the climatological sea ice albedo values used in ERA5 are not adequate and need revising, in order to better simulate surface heat
20 fluxes in the Arctic.

The advantage of the resulting broadband albedo data set from MERIS against other published data sets is the additional data set of melt pond fraction available from the same sensor. Melt ponds are the main reason for the sea ice albedo change in summer but currently are not represented in climate models. Additional information on melt evolution together with the accurate albedo product can aid the challenging representation of sea ice optical properties in summer in climate models.

The Cryosphere

Open Access

EGU

Discussions

1 Introduction

Broadband albedo of sea ice including the snow covered sea ice is a key parameter in Arctic climate studies. It is defined as the ratio of the reflected to incident irradiance in the waveband 200 - 5000 nm (Pedersen and Winther, 2005; Wendisch and Yang, 2012). The broadband albedo of sea ice determines the energy budget of the surface and controls the heat and mass balance of the sea ice cover (Perovich, 1994). Even small changes in the broadband albedo at surface can strongly influence the Arctic climate by the albedo-feedback mechanism. As broadband albedo of sea ice decreases, more radiation is absorbed at the surface, resulting in an increase of surface temperature and a loss of sea ice which amplifies the albedo reduction (Curry et al., 1995; Perovich et al., 2002; Pirazzini, 2008).

For a better understanding of the strong sensitivity of the Arctic climate to surface broadband albedo variations, climate studies need surface broadband albedo values which meet two criteria. Firstly, the surface broadband albedo has to be comprehensive in space and time to capture its strong variability with low albedo over melt ponds and high albedo over snow covered sea ice. Many surface broadband albedo data products from different satellite missions are available for this purpose. Table 1 provides an overview of the major ones and their specifications. The albedo data from MODerate resolution Imaging Spectroradiometer (MODIS) onboard Terra and Aqua (Lucht et al., 2000; Schaaf et al., 2002) has been widely used as a reference for evaluating other albedo products. The Polar Pathfinder-Extended (APP-x) climate data record from Advanced Very High Resolution Radiometer (AVHRR) measurements onboard various NOAA POES (U. S. National Oceanic and Atmospheric Administration Polar Operational Environmental Satellites) includes the first long-time series of consistent surface broadband albedo, starting from 1982 (Key et al., 2016). MERIS (Medium Resolution Imaging Spectrometer) onboard ENVISAT (ENVIronmental SATellite) provides the surface albedo of Arctic sea ice on a daily basis (Istomina et al., 2015). VIIRS (Visible Infrared Imaging Radiometer Suite) onboard S-NPP (Suomi National Polar-orbiting Partnership) belongs to the newest moderate spatial resolution imaging radiometers generating the surface albedo (He et al., 2018b). High spatial resolution surface albedo (30 m) at the expense of reduced temporal resolution (16 days) are generated by Operational Land Imager (OLI), Thematic Mapper (TM) and Enhanced Thematic Mapper Plus (ETM+) onboard Landsat satellites (He et al., 2018b). Furthermore, surface albedo can be retrieved from collaborative observations of multiple platforms, e. g. GlobAlbedo (Muller et al., 2012; Lewis et al., 2013) and Global land surface satellite (GLASS - Liu et al., 2013; Liang et al., 2013), or from radiation budget data sets, e. g. Clouds and the Earth's Radiant Energy System – Energy Balanced And Filled (CERES-EBAF, 2014; Loeb et al., 2018) and International Satellite Cloud Climatology Project (ISCCP – Zhang et al., 1995, 2004).

Secondly, the surface broadband albedo included in climate models has to fulfill an absolute accuracy of 0.02 – 0.05 as shown in sensitivity analysis (Henderson-Sellers and Wilson, 1983; Jacob and Olioso, 2005; Sellers et al., 1995). However, the satellite retrieved albedo products underlie uncertainties depending on the number and spectral distribution of satellite channels (i. e. narrowbands) available, on the temporal and spatial resolution of the measurement (Tab. 1), as well as on the approach to retrieve the broadband albedo (kernel driven BRDF (bidirectional reflectance distribution function) based methods or ARC (anisotropy reflectance correction) methods, both combined with a narrow-to-broadband conversion (NTBC), direct estimation methods, and methods using RTT (radiative transfer theory)) (Liang, 2001; Qu et al., 2014). Latter dependency is

caused by pre-assumed surface and atmospheric conditions in most retrieval methods whose representativeness to the actual ones determine the accuracy of the retrieved albedo product. Only the algorithm for MERIS data by Istomina et al. (2015) utilizes a physical model of sea ice in consideration of its melting stage and, therefore, does not depend on a priori assumptions of the surface and atmospheric conditions which can introduce an error in the retrieved albedo product.

5   However, the retrieval algorithm by Istomina et al. (2015) calculates the broadband albedo from MERIS data by averaging the MERIS derived spectral albedo at wavelengths $400, 500, 600, 700, 800,$ and 900 nm. Therefore, the MERIS derived broadband albedo covers the waveband 400 - 900 nm. It cannot be used in climate studies which usually need surface albedo values in the waveband $300 – 5000$ nm (He et al., 2018b) and is not comparable with other satellite derived broadband albedo products with wavebands larger than 300 - 3000 nm (Tab. 1). A comparison of surface broadband albedo products in different wavebands

10   reveals significant discrepancies which can exceed the required albedo accuracy in climate simulations (Li and Leighton, 1992; Winther et al., 2003; Bourgeois et al., 2006). The validation of MERIS derived broadband albedo against airborne measurements showed that over landfast ice the MERIS broadband albedo is higher by 0.06 on average than respective airborne measurements in the waveband $285 – 2800$ nm because of its lack of radiative information in the near infrared spectral region (Istomina et al., 2015).

15   In this paper, we introduce a spectral-to-broadband conversion (STBC) which replaces the conversion method proposed by Istomina et al. (2015) to calculate broadband albedo in the waveband $300 – 3000$ nm from spectral albedo retrieved from MERIS swath observations by the Melt Pond Detector (MPD) algorithm (Zege et al., 2015). With these new broadband albedo values, we improve the validation of the MPD algorithm by Istomina et al. (2015). The new MERIS broadband albedo can be used to evaluate and validate other albedo products from different satellite observations and to test albedo parameterizations in

20   climate models and atmospheric reanalyses. As the MPD algorithm additionally retrieves the melt pond fraction from MERIS observations, it is possible for the first time to include simultaneous derived broadband albedo values and melt pond fractions into climate models and atmospheric reanalyses.

After a short description of the MPD algorithm which derives spectral albedo and melt pond fraction of sea ice from MERIS observations, the empirically derived spectral-to-broadband conversion of the albedo is presented (Sect. 2). This conversion is

25   tested against proposed conversion techniques by Istomina et al. (2015) and Gao et al. (2004) in Sect. 3. The new broadband albedo of Arctic sea ice retrieved from MERIS observations is validated (Sect. 4). In Sect. 5, they are compared with respective values derived from the atmospheric reanalysis data set ERA5 produced by the European Centre for Medium-Range Weather Forecasts (Hersbach et al., 2018) to investigate the consistency of the sea ice albedo used in a state-of-the-art atmospheric reanalysis with satellite observations. Conclusions are given in Sect. 6.

30   For reasons of short expressions, the following sections always refer to albedo products at surface even if they are not explicitly declared as such.

2 Method

Broadband albedo over Arctic sea ice can be derived swathwise from MERIS observations in two steps. Firstly, spectral albedo is retrieved from MERIS swath Level 1b data over Arctic sea ice by the Melt Pond Detector (MPD) algorithm (Sect. 2.1). Secondly, these spectral albedo values have to be converted into broadband albedo values (Sect. 2.2).

2.1 Melt Pond Detector algorithm

The Melt Pond Detector (MPD) algorithm (Zege et al., 2015) derives spectral albedo at wavelengths $\lambda_i = 400, 500, 600, 700, 800,$ and 900 nm and melt pond fraction over Arctic sea ice from MERIS swath data. It contains a newly developed physical model of sea ice and melt pond reflection and takes into account the bidirectional reflectance of ice. The MPD algorithm is described in detail by Zege et al. (2015) and has been validated by Istomina et al. (2015). Input parameters are Level 1B data from MERIS onboard ENVISAT, including radiances of channels 1, 2, 3, 4, 8, 10, 12, 13, and 14 at center wavelengths 412.5, 442.5, 490, 510, 681.25, 753.75, 778.75, 865, and 885 nm, respectively, solar and observation angles. Relevant information about the atmospheric and surface state (atmosphere profile, aerosol load, borders for ice and pond optical properties) can be entered from an input file. Within the MPD algorithm, radiances reflected by sea ice are atmospherically corrected and used to derive ice and pond parameters (optical thickness of pond and ice, scattering coefficient of ice, effective ice grain size, and absorption coefficient of yellow pigments). From these parameters, the spectral albedo at the above mentioned wavelengths, the melt pond fraction, and the retrieval error for each sea ice pixel are calculated.

2.2 Broadband albedo conversion

The six spectral albedo values $\alpha(\lambda)$ at wavelengths $\lambda_i = 400, 500, 600, 700, 800,$ and 900 nm are converted in the MERIS broadband albedo by the linear combination:

$$\alpha_{bb} = k_0 + \sum_{i=1}^{6} k_i \cdot \alpha(\lambda_i). \tag{1}$$

The coefficients k_i of the spectral-to-broadband conversion (STBC) are empirically derived from spectral and broadband albedo values measured by Polashenski (2011) on landfast ice close to Barrow, AK, USA, between April and June of the years 2008 and 2009. The objective of the ground-based measurements was to investigate albedo and melt pond evolution during the melt season. The data are available at http://chrispolashenski.com/data.php.

Spectral and broadband albedo were measured along three 200 m long transect lines, orientated west-east and located on first-year sea ice 1 km offshore of Barrow, AK, USA (71.366 ° N, 156.542 ° W). The spectral albedo between 350 - 2500 nm was derived from upward and downward irradiance measurements using an Analytical Spectral Devices (ASD) spectrometer 'FieldSpec3' with a diffuse cosine collector. The broadband albedo in the waveband 300 – 3000 nm was measured by a Kipp&Zonen CM14 albedometer. Each of the two optics was mounted on a 1.5 m long arm and was positioned about 1 m above the surface (Polashenski, 2011).

Spectral and broadband albedo were measured along a first transect line on 21 days between April and June 2008. Along the second transect line, measurements were done on 13 days between May and June 2009 and along the third transect line on 12 days in June 2009. The second and third transect lines were 1 km apart of each other. The measurements were done once per day (except 14 June 2008 with twice per day) in steps of $2.5 – 5$ m under various sky conditions (clear, cloudy, and overcast skies). The time of spectral and broadband albedo measurements may differ by more than one hour because the spectral and broadband albedo samples were recorded one after the other.

After exclusion of unphysically high and discontinuous albedo spectra, 1720 albedo spectra and broadband albedo values of various sea ice surface types are available, from optically thick (snow depth $\gtrsim 10\,\text{cm}$) and thin snow (snow depth $\lesssim 10\,\text{cm}$), bare ice with loose decaying ice crystals on top, slushy bare ice to frozen and liquid melt ponds. Spatially and temporally collocated spectral and broadband albedo measurements were used to derive the coefficients k_i in Eq. (1) that minimize the square sum of errors $(\alpha_{\text{bb}} - k_0 - \sum_{i=1}^{6} k_i \cdot \alpha(\lambda_i))^2$, where k_0 was set to 0. The resulting coefficients are given in Tab. 2 and can be used to calculate the broadband albedo in waveband $300 – 3000$ nm. This method is referred to as empirically derived STBC.

3 Results

We investigate the performance of the empirically derived STBC (Sect. 3.1) and compare this new conversion to those methods proposed in Istomina et al. (2015) and Gao et al. (2004) (Sect. 3.2). For the evaluation, we used the root mean square deviation (RMSD) as an estimator for the statistic deviation, the mean difference of measured and retrieved albedo (bias) as an estimator for the systematic deviation, and the coefficient of determination (R^2) which allows conclusions about the quality of correlation. Measurement uncertainties in the considered data sets are neglected as they are relatively small compared to influences due to time offsets or different spatial resolutions of the measurements.

3.1 Regression analysis of the empirically derived STBC

The performance of the empirically derived STBC by using the training data set is presented in Fig. 1. It shows the broadband albedo measured by Polashenski (2011) over landfast ice close to Barrow, AK, USA between April and June of the years 2008 and 2009 and the broadband albedo product α_{bb} retrieved from the empirically derived STBC using respective spectral albedo values measured by Polashenski (2011). The combination of a high determination coefficient ($R^2 = 0.96$) and a low RMSD of 0.05 between the measured and the retrieved broadband albedo indicates a good performance of the empirically derived STBC. Systematic errors are not found (bias = 0.00). The slope of 0.93 and the intercept of 0.04 of the regression line indicate a slight overestimation of low albedo values and a slight underestimation of high albedo values by the empirically derived STBC.

Note, that the deviations between measured and retrieved broadband albedo are not only caused by the empirically derived STBC but also by time offsets between the measured spectral and broadband albedo. Within this time difference, the prevailing illumination can be significantly modified due to changes in the solar zenith angle and cloud conditions. As a result, nonconforming spectral and broadband albedo values were measured.

Coefficients k_i derived separately for each surface type mentioned at the end of Sect. 2.2 and a surface specific application of those (Eq. 1) do not improve the results given in Fig. 1 (not shown).

3.2 Comparison to existing conversion methods

The empirically derived STBC is compared with conversion methods proposed in Istomina et al. (2015) and Gao et al. (2004).
5 Their coefficients k_i are listed in Tab. 2. Istomina et al. (2015) calculated broadband albedo by averaging the spectral albedo values. Gao et al. (2004) propose a linear combination method of albedo values from MERIS channels 3, 5, 7, and 13 at the center wavelengths $\lambda_i^* = 490, 560, 665$, and 865 nm instead of λ_i. The coefficients k_i in Gao et al. (2004) were adopted from the narrow to broadband conversion developed for albedo values from MISR (multi-angle imaging spectrometer) onboard Terra satellite by (Liang et al., 1999). This conversion is based on radiative transfer simulations.

10 For the comparison, an independent test data set of measured spectral and broadband albedo was obtained as part of the ACLOUD (Arctic CLoud Observations Using airborne measurements during polar Day) campaign (Wendisch et al., in press). The measured spectral albedo is available in Jäkel et al. (2018), details on measured broadband albedo are given in Jäkel et al. (2019). The meteorological conditions during the campaign are documented in Knudsen et al. (2018). On 25 June 2017, spectral and broadband albedo were measured on board of aircraft Polar 5 north of Svalbard (80.48 ° – 81.62 ° N, 11.31 ° –
15 20.36 ° E). The measurements were done over sea ice floes of different sizes under cloud free conditions. The flight altitude of the selected flight sections was between 50 and 200 m.

Spectral albedo was derived from hemispheric up- and downwelling spectral radiation detected by SMART (Spectral Modular Airborne Radiation Measurement System) in the wavelength range $350 – 2200$ nm within an accuracy of 10 %. SMART was actively stabilized in a horizontal position (Wendisch et al., 2001; Ehrlich et al., 2008; Bierwirth et al., 2009). The tempo-
20 ral resolution of the spectral measurements was 2 Hz. Broadband albedo in waveband $200 – 3600$ nm was measured by two Kipp&Zonen CMP-22 pyranometers within an error of 3 %, as given by the manufacturer for stationary operation. Both pyranometers were mounted in a fixed position at the top and at the bottom of the aircraft's fuselage for a simultaneous detection of the hemispheric down- and upwelling radiation. The temporal sampling interval was increased to 20 Hz by the deconvolution method described in Ehrlich and Wendisch (2015). For clear-sky conditions, the measurements of the upward-facing pyra-
25 nometer were corrected for deviations from horizontal attitude due to misalignment of the instrument and roll and pitch angles of the aircraft based on a method given by Bannehr and Schwiesow (1993) and described in Lampert et al. (2012). Broadband measurements at roll and pitch angles higher than 4 ° are excluded.

The broadband albedo measured during ACLOUD covers a wider wavelength range ($200 – 3600$ nm) than the broadband albedo which is calculated by the empirically derived STBC ($300 – 3000$ nm). Resulting discrepancies between both albedo
30 products due to the different wavebands are estimated by the radiative transfer model libRadtran (Mayer and Kylling, 2005) and are lower than 0.01. Those systematic errors are negligible when comparing both broadband albedo products.

Spectral and broadband albedo values were temporally adjusted. Influences caused by their different sampling intervals (2 Hz and 20 Hz) were diminished by convolving the broadband albedo values by a running average of 10 measurements.

In Fig. 2, measured broadband albedo is compared to the broadband albedo α_{bb} retrieved by the empirically derived STBC using spectral albedo measured by SMART. Retrieved and measured broadband albedo are highly correlated ($R^2 = 0.98$). The regression slope of 1.06 is close to 1 and together with the -0.03 intercept causes a small underestimation of low albedo values. Discrepancies between both broadband albedo products ($\mathrm{RMSD} = 0.02$) are caused by uncertainties in the empirically

5   derived STBC (Fig. 1) as well as by measurement uncertainties in the spectral and broadband albedo. Another reason can be the sky condition. Most of the albedo measurements used for the empirical development of the STBC were cloud contaminated. Clouds can slightly increase the broadband albedo of snow by up to 0.06 (Key et al., 2001; Grenfell and Perovich, 1984) and, therefore, influences the empirical derivation of the STBC. This cloud contaminated STBC is applied here to albedo measurements under clear-sky conditions which can contribute to the discrepancies shown in Fig. 2. However, an empirical

10   derivation of the coefficients in Eq. (1) using only albedo measurements under clear-sky conditions (113 albedo spectra and broadband albedo values) by Polashenski (2011) and an application of those to the albedo measurements during ACLOUD deteriorate the results given in Fig. 2 (not shown).

For comparison, Fig. 3 shows measured broadband albedo and respective retrieved broadband albedo α_{bb} with conversion methods proposed in Istomina et al. (2015) and Gao et al. (2004), respectively. Retrieved broadband albedo values of both

15   conversions correlate well with measured broadband albedo values ($R^2 = 0.98$ in both cases). But the conversion from Istomina et al. (2015) overestimates the broadband albedo (mean difference of $\mathrm{bias} = -0.08$) while the conversion from Gao et al. (2004) underestimates it ($\mathrm{bias} = 0.04$). Accordingly, RMSD values (0.09 and 0.05) are higher than for the empirically derived STBC.

4   Improved Melt Pond Detector Validation

The MPD algorithm by Zege et al. (2015) is combined with the empirically derived STBC to retrieve more accurate broadband

20   albedo values of Arctic sea ice from MERIS observations compared to the procedure described in Istomina et al. (2015). With these new values, we will improve the validation of the MPD algorithm performed in Istomina et al. (2015).

The new MERIS broadband albedo product is validated with measured broadband albedo during the aircraft campaign MELTEX (Impact of melt ponds on energy and momentum fluxes between atmosphere and sea ice) performed by the Alfred Wegener Institute, Helmholtz Centre for Polar and Marine Research (AWI) over the southern Beaufort Sea between May and

25   June 2008. The goal of the campaign was to improve the quantitative understanding of the impact of melt ponds on radiation, heat and momentum fluxes over Arctic sea ice (Birnbaum et al., 2009).

To determine the broadband albedo, two Eppley Precision Spectral Pyranometers were mounted on aircraft Polar 5 in a fixed position measuring simultaneously the hemispheric down- and upwelling radiation integrated over the waveband from 285 to 2800 nm. Analogous to the broadband measurements during ACLOUD, the measurements of downwelling radiation at clear-

30   sky conditions were corrected for deviations from horizontal attitude based on the method given by Bannehr and Schwiesow (1993).

On five days (26 May, 3, 4, 6, and 7 June 2008), airborne broadband albedo was measured under almost clear-sky conditions. Measurement times are given in Tab. 3. Maps of flight tracks are shown in Birnbaum et al. (2009). The flight altitude was

between 50 and 400 m. On 6 June, broadband albedo was measured over landfast ice, on the other selected days measurements were performed over drifting ice with ice floes of different sizes.

Due to two warming events between 23 – 24 May and 1 – 7 June, broadband albedo was measured over sea ice at different melting stages: On 26 May and 3 June, melt ponds at early stages were overflown, on 4 June the snow was either melted away

5   or was very wet and the number and size of melt ponds rose. On 6 and 7 June, the observed sea ice was homogeneously covered by well developed melt ponds.

Airborne measured broadband albedo is collocated with MERIS broadband albedo derived for each pixel from MERIS swath data at reduced resolution of 1.2 km. The MERIS overflight times which corresponds to the airborne flights are also given in Tab. 3. The time difference between the airborne and satellite measurements stays below 2 hours except for 3 and 7 June with

10 a maximum difference of 3 and 4 hours, respectively.

For the collocation of airborne and MERIS broadband albedo, the orthodromic distance between each MERIS pixel center and the location of a given airborne measurement is calculated. Each airborne measurement is allocated to that satellite pixel with the least orthodromic distance. Depending on orientation and location of flight track as well as MERIS pixel availability, up to 14 airborne broadband albedo measurements are collocated to one MERIS derived broadband albedo value. The airborne

15 broadband albedo values are averaged for each satellite pixel.

The scatterplots in Figs. 4 and 5 show the correlation of the MERIS derived and collocated airborne broadband albedo for measurements over landfast ice and over drift ice, respectively. Collocated airborne and MERIS broadband albedo values are used for validation only if more than five airborne broadband albedo values are available for one MERIS pixel. Time differences between airborne and MERIS measurements up to 1.5 h were allowed.

20 For the landfast ice case (Fig. 4), MERIS broadband albedo is slightly higher at low albedo values than the corresponding airborne broadband albedo. For drift ice cases (Fig. 5), the respective overestimation is higher and an underestimation at high albedo values occurs (slope $= 0.53$, intercept $= 0.25$).

The highest correlation and lowest RMSD value is found for broadband albedo values over landfast ice on 6 June 2008 ($R^2 = 0.93$, RMSD $= 0.04$). Compared to landfast ice, the RMSD $= 0.07$ for the drifting ice cases (Fig. 5) is nearly twice as

25 high and the correlation is lower ($R^2 = 0.78$). Correlation and RMSD values depend on weather conditions, ice concentration, surface inhomogeneity, time differences between satellite overflight and airborne measurements, and spatial resolution of the observation. As landfast ice is stationary over long time, airborne measurements are not displaced relative to satellite measurements during the time lag between both observations. Over drifting ice floes at lower sea ice concentrations, a higher sea ice drift can be expected (free drift conditions). Therefore, the surface conditions observed by aircraft and satellite can get

30 more different (compare the three outliers at low measured albedo values in Fig. 5). The discrepancies between MERIS derived and airborne broadband albedo values are increased by their different spatial resolution which depends on observation heights and instrument optics. As clearly seen in the histogram in Fig. 5 the sparser spatial resolution of MERIS observations lead to a lower albedo variability compared to the respective airborne measurements. Moreover, the bimodal albedo distribution shown in the airborne measurements are smeared out in the respective satellite retrievals. For the landfast ice case, the surface

conditions are more homogeneous and thus the difference in spatial resolution has less influence on the comparison (see histogram in Fig. 4).

In contrast, the validation of MERIS broadband albedo values derived by the procedure described in Istomina et al. (2015), i. e. the combination of the MPD algorithm and the spectral averaging method by coefficients given in Tab. 2, results in similar correlation values of $R^2 = 0.94$ for the landfast ice case and $R^2 = 0.78$ for the drift ice cases. The RMSDs are 0.06 (landfast ice) and 0.09 (drift ice) and thus exceed the values found above. This again illustrates the better performance of the empirically developed STBC compared to the spectral averaging method proposed in Istomina et al. (2015).

5 Comparison between broadband albedo from satellite and atmospheric reanalysis

During the melt season in Arctic summer, the Arctic sea ice experiences rapid changes in the albedo mainly caused by the melt pond development (Eicken et al., 2002; Polashenski, 2011). As the melt pond fraction on sea ice evolves according to the sequence of melt stages (Eicken et al., 2002), information on the melt pond fraction and knowledge on the melt evolution can improve the current representation of the summer energy balance in climate models and atmospheric reanalyses, especially in the situations where accurate albedo representation is challenging.

At the time of writing, there is no published reference of melt ponds assimilated into any climate model or atmospheric reanalysis. Therefore, we only perform an albedo comparison in this work with the objective of testing the albedo parameterization used in ERA5. ERA5 is the fifth generation of climate reanalysis data sets produced by ECMWF. It provides hourly values of atmospheric and land variables from 1950 onwards with a spatial resolution of 31 km, obtained by an ensemble 4D-Var data assimilation system (Hersbach et al., 2018).

Although a vast amount of satellite and in-situ observations are assimilated in ERA5, the sea ice surface albedo is simply prescribed as constants following the parametrized albedo values by Ebert and Curry (1993). The ERA5 sea ice albedo is representative for dry snow during the months September to May, representative for melting snow in June, and representative for bare sea ice in July and August. Melt ponds are not represented at any time. The Ebert & Curry values are taken to be valid at the 15th day of the month, and the values for all other days are obtained by linear interpolation. The grid-cell albedo for ERA5 is then a linear combination between this sea ice albedo, and the open water albedo:

$$\alpha_{\mathrm{ERA5}} = \alpha_{\mathrm{seaice}} \cdot c + \alpha_{\mathrm{water}} \cdot (1 - c) \quad . \tag{2}$$

The effective grid-cell broadband albedo of ERA5 can be calculated from hourly averaged (h) ERA5 net and downward irradiances $F_{\mathrm{net}}(h)$ and $F_{\mathrm{dn}}(h)$ at surface in the waveband $200 - 4000$ nm. Thus, daily averaged ERA5 broadband albedo is given by:

$$\alpha_{\mathrm{ERA5}} = 1 - \frac{\sum_{h=0}^{23} F_{\mathrm{net}}(h)}{\sum_{h=0}^{23} F_{\mathrm{dn}}(h)} \quad . \tag{3}$$

F_{net} and F_{dn} were generated by using Copernicus Climate Change Service (2017).

Figure 6 shows daily averaged ERA5 and MERIS broadband albedo of Arctic sea ice together with their differences for three days in June 2007, respectively. Cloud contaminated grid cells in MERIS data are flagged by MPD algorithm and are removed. On 2 June 2007, just a few days before melt onset, ERA5 broadband albedo values are similar to respective MERIS albedo values south of a geographical latitude of 78 ° N except in the Chukchi Sea and East Siberian Sea where the ERA5 broadband albedo is higher by up to 0.20. From 78 ° N towards the North Pole, ERA5 broadband albedo is smaller than the MERIS broadband albedo by up to 0.16. On 12 June 2007, the melting season has started between 120 ° W and 120 ° E which is clearly visible by lower and similar ERA5 and MERIS broadband albedo values (0.30 − 0.60). North of Greenland, the Fram Strait, and Svalbard, ERA5 broadband albedo remains lower compared to MERIS by values up to 0.18. Best agreement between ERA5 and MERIS broadband albedo is achieved on 25 June 2007, after melting has started in the whole Arctic with differences below ± 0.10.

Scatterplots of both albedo products for the selected days are shown in Fig. 7. The correlation of MERIS and ERA5 broadband albedo is between 0.71 and 0.77. The point clusters indicate that in most of the cases high broadband albedo values from ERA5 are lower than respective values from MERIS observations whereas medium albedo values from ERA5 and MERIS observations are similar. The $\text{RMSD} = 0.12$ is more than twice higher than the accuracy required for climate studies (0.02 - 0.05). The minimum ERA5 broadband albedo is 0.05. The MERIS broadband albedo can be even lower down to 0. The large fraction of very low MERIS broadband albedo values, however, can be incorrectly caused by sea ice edge effects where spectral albedo derivation with MPD algorithm might fail.

The vertical orientation of the cluster borders at high ERA5 broadband albedo values on 12 and 25 June and the minimum achievable albedo of 0.05 in ERA5 are caused by the albedo parameterization in the Integrated Forecasting System (IFS) (Eq. 2). According to the linear dependency of the albedo α_{ERA5} on the ice concentration c, the minimum and maximum achievable albedo are restricted to the albedo of water $\alpha_{\text{water}} = 0.05$ ($c = 0$) and the albedo of sea ice α_{seaice} ($c = 1$).

6 Conclusions

In this study, a spectral to broadband conversion (STBC) has been developed empirically which can be used in combination with the Melt Pond Detector (MPD) algorithm (Zege et al., 2015) to derive broadband albedo (300 - 3000 nm) of Arctic sea ice from MERIS swath data. The empirically derived STBC has been developed with spectral and broadband albedo measured over landfast ice close to Barrow, AK, USA between April and June of the years 2008 and 2009 (Polashenski, 2011). It has been validated with airborne measured spectral and broadband albedo of drifting sea ice north of Svalbard on 25 June 2017 (Wendisch et al., in press). Compared to the measured broadband albedo, the empirically derived STBC calculates broadband albedo with a low root mean square deviation (RMSD) of 0.02 and a high correlation of 0.98. However, low albedo values are slightly underestimated. It performs more accurate then conversions proposed by Istomina et al. (2015) and Gao et al. (2004) which results in RMSDs of 0.09 and 0.05, respectively.

The empirically derived STBC replaces the spectral averaging method proposed by Istomina et al. (2015) in the derivation of broadband albedo from MERIS swath data. The new obtained broadband albedo values improve the validation of the MPD algorithm with respective airborne measurements over the southern Beaufort Sea between May and June 2008 (Birnbaum et al., 2009). The RMSD varies between 0.04 for landfast ice and 0.07 for drift ice. Both RMSDs are 0.02 lower than those when

5   using the conversion method by Istomina et al. (2015). The higher RMSD for drift ice can result from the sea ice drift which displaces the airborne measurements relative to satellite observations during the time lag between both measurements. Another reason is the different spatial resolution of airborne and satellite measurements in combination with the more inhomogeneous surface condition of drift ice relative to landfast ice.

The new MERIS derived broadband albedo of sea ice has been compared with respective albedo values retrieved from

10   atmospheric reanalysis data set ERA5 (ECMWF, 2019) to test the albedo parameterization used in ERA5. The RMSD between both data sets of 0.12 exceeds the required absolute accuracy of 0.02 - 0.05 in climate models (Henderson-Sellers and Wilson, 1983; Jacob and Olioso, 2005; Sellers et al., 1995). At moderate albedo values, the discrepancy between ERA5 and MERIS broadband albedo is lower than ± 0.10. High albedo values are lower by up to 0.18 compared to the MERIS albedo. Latter is caused by the albedo parameterization which limits the ERA5 albedo to the top by the literature based albedo of bare sea

15   ice, dry and melting snow. Hence, the constant sea ice albedo values used in ERA5 are not suited to simulate the observed variability and change in sea ice albedo. As an interim solution, prognostic modeling schemes of sea ice albedo should be developed, which can be validated against observational products like the MERIS derived broadband albedo presented here. It might be desirable to assimilate satellite derived sea ice albedo when producing an atmospheric reanalysis. MERIS derived broadband albedo can be useful in this context, because it is not based on a priori values and is available daily even though

20   only at daylight and under cloud free conditions.

The empirically derived STBC has been developed based on an albedo data set measured under clear-sky, cloudy, and overcast conditions. However, clouds increase the broadband albedo of snow by 0.06 (Key et al., 2001; Grenfell and Perovich, 1984). Thus, clouds affect the accuracy of the empirically derived STBC which may contribute to uncertainties in converting spectral to broadband albedo under clear-sky conditions, i. e. the only conditions when satellite data is available. The influence

25   of this uncertainty on the satellite albedo retrieval needs further investigations. Radiative transfer simulations can be a beneficial approach in this context because they offer more flexible and specific set-ups of surface, atmosphere, and cloud types as available in short term campaigns. Another advantage of radiative transfer simulations is the possibility to calculate the different radiometric parameters for the same meteorological situation whereas measurements are done within a certain time frame in which the meteorological situation can rigorously change.

30   The combination of the MPD algorithm and the empirically derived STBC allows to derive broadband albedo for the complete Arctic sea ice cover under cloud free conditions between March 2002 and April 2012 from MERIS swath data. This 10 years long data set can be used with the additional melt pond fraction data in Arctic climate investigations, for evaluation, validation, and data assimilation purposes, as well as in comparative studies. As a next step, swath data from OLCI (Ocean and Land Color Instrument) onboard SENTINEL-3 will be implemented in the MPD algorithm to extend the broadband albedo

35   time series of Arctic sea ice from 2016 up to date.

References

Bannehr, L. and Schwiesow, R.: A Technique to Account for the Misalignment of Pyranometers Installed on Aircraft, Journal of Atmospheric and Oceanic Technology, 10, 774–777, https://doi.org/10.1175/1520-0426(1993)010<0774:ATTAFT>2.0.CO;2, https://doi.org/10.1175/1520-0426(1993)010<0774:ATTAFT>2.0.CO;2, 1993.

5 Bierwirth, E., Wendisch, M., Ehrlich, A., Heese, B., Tesche, M., Althausen, D., Schladitz, A., MüLLER, D., Otto, S., Trautmann, T., Dinter, T., Hoyningen-HUENE, W. V., and Kahn, R.: Spectral surface albedo over Morocco and its impact on radiative forcing of Saharan dust, Tellus B: Chemical and Physical Meteorology, 61, 252–269, https://doi.org/10.1111/j.1600-0889.2008.00395.x, https://doi.org/10.1111/j.1600-0889.2008.00395.x, 2009.

Birnbaum, G., Dierking, W., Hartmann, J., Lüpkes, C., Ehrlich, A., Garbrecht, T., and Sellmann, L.: The campaign MELTEX with research

10 aircraft "POLAR 5" in the Arctic in 2008, Berichte zur Polar-und Meeresforschung (Reports on Polar and Marine Research), 593, 2009.

Bourgeois, C. S., Calanca, P., and Ohmura, A.: A field study of the hemispherical directional reflectance factor and spectral albedo of dry snow, Journal of Geophysical Research: Atmospheres, 111, https://doi.org/10.1029/2006JD007296, https://agupubs.onlinelibrary.wiley.com/doi/abs/10.1029/2006JD007296, 2006.

CERES-EBAF: CERES_EBAF_Ed2.8 Data Quality Summary, https://ceres.larc.nasa.gov/documents/DQ_summaries/CERES_EBAF_Ed2.

15 8_DQS.pdf, 2014.

Copernicus Climate Change Service: ERA5: Fifth generation of ECMWF atmospheric reanalyses of the global climate. Copernicus Climate Change Service Climate Data Store (CDS), https://cds.climate.copernicus.eu/cdsapp#!/home, 2018-11-19, 2017.

Curry, J. A., Schramm, J. L., and Ebert, E. E.: Sea Ice-Albedo Climate Feedback Mechanism, Journal of Climate, 8, 240–247, https://doi.org/10.1175/1520-0442(1995)008<0240:SIACFM>2.0.CO;2, https://doi.org/10.1175/1520-0442(1995)008<0240:SIACFM>

20 2.0.CO;2, 1995.

Ebert, E. E. and Curry, J. A.: An intermediate one-dimensional thermodynamic sea ice model for investigating ice-atmosphere interactions, Journal of Geophysical Research: Oceans, 98, 10 085–10 109, https://doi.org/10.1029/93JC00656, https://agupubs.onlinelibrary.wiley.com/doi/abs/10.1029/93JC00656, 1993.

ECMWF: ERA5, https://www.ecmwf.int/en/forecasts/datasets/archive-datasets/reanalysis-datasets/era5, 2019-01-18, 2019.

25 Ehrlich, A. and Wendisch, M.: Reconstruction of high-resolution time series from slow-response broadband terrestrial irradiance measurements by deconvolution, Atmospheric Measurement Techniques, 8, 3671–3684, https://doi.org/10.5194/amt-8-3671-2015, https://www.atmos-meas-tech.net/8/3671/2015/, 2015.

Ehrlich, A., Bierwirth, E., Wendisch, M., Gayet, J.-F., Mioche, G., Lampert, A., and Heintzenberg, J.: Cloud phase identification of Arctic boundary-layer clouds from airborne spectral reflection measurements: test of three approaches, Atmospheric Chemistry and Physics, 8,

30 7493–7505, https://doi.org/10.5194/acp-8-7493-2008, https://www.atmos-chem-phys.net/8/7493/2008/, 2008.

Eicken, H., Krouse, H. R., Kadko, D., and Perovich, D. K.: Tracer studies of pathways and rates of meltwater transport through Arctic summer sea ice, Journal of Geophysical Research: Oceans, 107, SHE 22–1–SHE 22–20, https://doi.org/10.1029/2000JC000583, https://agupubs.onlinelibrary.wiley.com/doi/abs/10.1029/2000JC000583, 2002.

Gao, F., Schaaf, C., Jin, Y.-F., Lucht, W., and Strahler, A.: Deriving albedo from coupled MERIS and MODIS surface products, 2004.

35 Grenfell, T. C. and Perovich, D. K.: Spectral albedos of sea ice and incident solar irradiance in the southern Beaufort Sea, Journal of Geophysical Research, 89, 3573–3580, https://doi.org/10.1029/JC089iC03p03573, 1984.

He, T., Liang, S., Wang, D., Cao, Y., Gao, F., Yu, Y., and Feng, M.: Evaluating land surface albedo estimation from Landsat MSS, TM, ETM+, and OLI data based on the unified direct estimation approach, Remote Sensing of Environment, 204, 181–196, https://doi.org/https://doi.org/10.1016/j.rse.2017.10.031, http://www.sciencedirect.com/science/article/pii/S0034425717304947, 2018a.

He, T., Wang, D., and Qu, Y.: Land Surface Albedo, 2018b.

5 Henderson-Sellers, A. and Wilson, M. F.: Surface albedo data for climatic modeling, Reviews of Geophysics, 21, 1743–1778, https://doi.org/10.1029/RG021i008p01743, https://agupubs.onlinelibrary.wiley.com/doi/abs/10.1029/RG021i008p01743, 1983.

Hersbach, H., de Rosnay, P., Bell, B., Schepers, D., Simmons, A., Soci, C., Abdalla, S., Alonso-Balmaseda, M., Balsamo, G., Bechtold, P., Berrisford, P., Bidlot, J.-R., de Boisséson, E., Bonavita, M., Browne, P., Buizza, R., Dahlgren, P., Dee, D., Dragani, R., Diamantakis, M., Flemming, J., Forbes, R., Geer, A. J., Haiden, T., Hólm, E., Haimberger, L., Hogan, R., Horányi, A., Janiskova, M., Laloyaux, P., Lopez,

10 P., Munoz-Sabater, J., Peubey, C., Radu, R., Richardson, D., Thépaut, J.-N., Vitart, F., Yang, X., Zsótér, E., and Zuo, H.: Operational global reanalysis: progress, future directions and synergies with NWP, https://doi.org/10.21957/tkic6g3wm, https://www.ecmwf.int/node/18765, 2018.

Istomina, L., Heygster, G., Huntemann, M., Schwarz, P., Birnbaum, G., Scharien, R., Polashenski, C., Perovich, D., Zege, E., Malinka, A., Prikhach, A., and Katsev, I.: Melt pond fraction and spectral sea ice albedo retrieval from MERIS data – Part 1: Validation against in

15 situ, aerial, and ship cruise data, The Cryosphere, 9, 1551–1566, https://doi.org/10.5194/tc-9-1551-2015, https://www.the-cryosphere.net/9/1551/2015/, 2015.

Jacob, F. and Olioso, A.: Derivation of diurnal courses of albedo and reflected solar irradiance from airborne POLDER data acquired near solar noon, Journal of Geophysical Research: Atmospheres, 110, https://doi.org/10.1029/2004JD004888, https://agupubs.onlinelibrary.wiley.com/doi/abs/10.1029/2004JD004888, 2005.

20 Jäkel, E., Ehrlich, A., Schäfer, M., and Wendisch, M.: Aircraft measurements of up- and downward irradiances over Arctic sea ice during the ACLOUD campaign, https://doi.org/10.1594/PANGAEA.891588, https://doi.org/10.1594/PANGAEA.891588, 2018.

Jäkel, E., Stapf, J., Wendisch, M., Nicolaus, M., Dorn, W., and Rinke, A.: Validation of the sea ice surface albedo scheme of the regional climate model HIRHAM–NAOSIM using aircraft measurements during the ACLOUD/PASCAL campaigns, The Cryosphere Discussions, 2019, 1–21, https://doi.org/10.5194/tc-2018-266, https://www.the-cryosphere-discuss.net/tc-2018-266/, 2019.

25 Key, J., Wang, X., Liu, Y., Dworak, R., and Letterly, A.: The AVHRR Polar Pathfinder Climate Data Records, Remote Sensing, 8, https://doi.org/10.3390/rs8030167, http://www.mdpi.com/2072-4292/8/3/167, 2016.

Key, J. R., Wang, X., Stoeve, J. C., and Fowler, C.: Estimating the cloudy-sky albedo of sea ice and snow from space, Journal of Geophysical Research: Atmospheres, 106, 12 489–12 497, https://doi.org/10.1029/2001JD900069, https://agupubs.onlinelibrary.wiley.com/doi/abs/10.1029/2001JD900069, 2001.

30 Knudsen, E. M., Heinold, B., Dahlke, S., Bozem, H., Crewell, S., Gorodetskaya, I. V., Heygster, G., Kunkel, D., Maturilli, M., Mech, M., Viceto, C., Rinke, A., Schmithüsen, H., Ehrlich, A., Macke, A., Lüpkes, C., and Wendisch, M.: Meteorological conditions during the ACLOUD/PASCAL field campaign near Svalbard in early summer 2017, Atmospheric Chemistry and Physics, 18, 17 995–18 022, https://doi.org/10.5194/acp-18-17995-2018, https://www.atmos-chem-phys.net/18/17995/2018/, 2018.

Lampert, A., Maturilli, M., Ritter, C., Hoffmann, A., Stock, M., Herber, A., Birnbaum, G., Neuber, R., Dethloff, K., Orgis, T., Stone,

35 R. S., Brauner, R., Kässbohrer, J., Haas, C., Makshtas, A., Sokolov, V., and Liu, P.: The Spring-Time Boundary Layer in the Central Arctic Observed during PAMARCMiP 2009, Atmosphere, 3, 320–351, https://doi.org/10.3390/atmos3030320, http://www.mdpi.com/2073-4433/3/3/320, 2012.

Lewis, P., Brockmann, C., Danne, O., Fischer, J., Guanter, L., Heckel, A., Krueger, O., Lopez, G., Muller, J. P., North, P., Potts, D., and Preusker, P.: GlobAlbedo: Algorithm theoretical basis document (V4.12), http://www.globalbedo.org/docs/GlobAlbedo_Albedo_ATBD_V4.12.pdf, 2013.

Li, Z. and Leighton, H. G.: Narrowband to Broadband Conversion with Spatially Autocorrelated Reflectance Measurements, Journal of Applied Meteorology, 31, 421–432, https://doi.org/10.1175/1520-0450(1992)031<0421:NTBCWS>2.0.CO;2, https://doi.org/10.1175/1520-0450(1992)031<0421:NTBCWS>2.0.CO;2, 1992.

Liang, S.: Narrowband to broadband conversions of land surface albedo I: Algorithms, Remote Sensing of Environment, 76, 213–238, https://doi.org/https://doi.org/10.1016/S0034-4257(00)00205-4, http://www.sciencedirect.com/science/article/pii/S0034425700002054, 2001.

Liang, S., Strahler, A. H., and Walthall, C.: Retrieval of Land Surface Albedo from Satellite Observations: A Simulation Study, Journal of Applied Meteorology, 38, 712–725, https://doi.org/10.1175/1520-0450(1999)038<0712:ROLSAF>2.0.CO;2, https://doi.org/10.1175/1520-0450(1999)038<0712:ROLSAF>2.0.CO;2, 1999.

Liang, S., Zhao, X., Liu, S., Yuan, W., Cheng, X., Xiao, Z., Zhang, X., Liu, Q., Cheng, J., Tang, H., Qu, Y., Bo, Y., Qu, Y., Ren, H., Yu, K., and Townshend, J.: A long-term Global LAnd Surface Satellite (GLASS) data-set for environmental studies, International Journal of Digital Earth, 6, 5–33, https://doi.org/10.1080/17538947.2013.805262, https://doi.org/10.1080/17538947.2013.805262, 2013.

Liu, Q., Wang, L., Qu, Y., Liu, N., Liu, S., Tang, H., and Liang, S.: Preliminary evaluation of the long-term GLASS albedo product, International Journal of Digital Earth, 6, 69–95, https://doi.org/10.1080/17538947.2013.804601, https://doi.org/10.1080/17538947.2013.804601, 2013.

Loeb, N. G., Doelling, D. R., Wang, H., Su, W., Nguyen, C., Corbett, J. G., Liang, L., Mitrescu, C., Rose, F. G., and Kato, S.: Clouds and the Earth's Radiant Energy System (CERES) Energy Balanced and Filled (EBAF) Top-of-Atmosphere (TOA) Edition-4.0 Data Product, Journal of Climate, 31, 895–918, https://doi.org/10.1175/JCLI-D-17-0208.1, https://doi.org/10.1175/JCLI-D-17-0208.1, 2018.

Lucht, W., Schaaf, C. B., and Strahler, A. H.: An algorithm for the retrieval of albedo from space using semiempirical BRDF models, IEEE Transactions on Geoscience and Remote Sensing, 38, 977–998, https://doi.org/10.1109/36.841980, 2000.

Mayer, B. and Kylling, A.: Technical note: The libRadtran software package for radiative transfer calculations - description and examples of use, Atmospheric Chemistry and Physics, 5, 1855–1877, https://doi.org/10.5194/acp-5-1855-2005, https://www.atmos-chem-phys.net/5/1855/2005/, 2005.

Muller, J.-P., López, G., Watson, G., Shane, N., Kennedy, T., Yuen, P., and Lewis, P.: The ESA Globalbedo Project for Mapping the Earth's Land Surface Albedo for 15 Years from European Sensors, http://www.mssl.ucl.ac.uk/~pcy/papers/Muller-GlobAlbedo-abstractV4.pdf, 2012.

Pedersen, C. A. and Winther, J.-G.: Intercomparison and validation of snow albedo parameterization schemes in climate models, Climate Dynamics, 25, 351–362, https://doi.org/10.1007/s00382-005-0037-0, https://doi.org/10.1007/s00382-005-0037-0, 2005.

Perovich, D. K.: Light reflection from sea ice during the onset of melt, Journal of Geophysical Research: Oceans, 99, 3351–3359, 1994.

Perovich, D. K., Grenfell, T. C., Light, B., and Hobbs, P. V.: Seasonal evolution of the albedo of multiyear Arctic sea ice, Journal of Geophysical Research: Oceans, 107, SHE 20–1–SHE 20–13, https://doi.org/10.1029/2000JC000438, https://agupubs.onlinelibrary.wiley.com/doi/abs/10.1029/2000JC000438, 2002.

Pirazzini, R.: Factors controlling the surface energy budget over snow and ice, Finnish Meteorolog. Inst. Contributions, 75, 2008.

Polashenski, C. M.: Attributing change and understanding melt ponds on a seasonal ice cover, Ph.D. thesis, Darthmouth College, Hanover, New Hampshire, 181 pp., 2011.

15

Qu, Y., Liu, Q., Liang, S., Wang, L., Liu, N., and Liu, S.: Direct-Estimation Algorithm for Mapping Daily Land-Surface Broadband Albedo From MODIS Data, IEEE Transactions on Geoscience and Remote Sensing, 52, 907–919, https://doi.org/10.1109/TGRS.2013.2245670, 2014.

Schaaf, C. B., Gao, F., Strahler, A. H., Lucht, W., Li, X., Tsang, T., Strugnell, N. C., Zhang, X., Jin, Y., Muller, J.-P., Lewis, P., Barnsley, M., Hobson, P., Disney, M., Roberts, G., Dunderdale, M., Doll, C., d'Entremont, R. P., Hu, B., Liang, S., Privette, J. L., and Roy, D.: First operational BRDF, albedo nadir reflectance products from MODIS, Remote Sensing of Environment, 83, 135–148, https://doi.org/https://doi.org/10.1016/S0034-4257(02)00091-3, http://www.sciencedirect.com/science/article/pii/S0034425702000913, the Moderate Resolution Imaging Spectroradiometer (MODIS): a new generation of Land Surface Monitoring, 2002.

Schiffer, R. A. and Rossow, W. B.: The International Satellite Cloud Climatology Project (ISCCP): The First Project of the World Climate Research Programme, Bulletin of the American Meteorological Society, 64, 779–784, https://doi.org/10.1175/1520-0477-64.7.779, https://doi.org/10.1175/1520-0477-64.7.779, 1983.

Sellers, P., Meeson, B., Hall, F., Asrar, G., Murphy, R., Schiffer, R., Bretherton, F., Dickinson, R., Ellingson, R., Field, C., Huemmrich, K., Justice, C., Melack, J., Roulet, N., Schimel, D., and Try, P.: Remote sensing of the land surface for studies of global change: Models — algorithms — experiments, Remote Sensing of Environment, 51, 3–26, https://doi.org/https://doi.org/10.1016/0034-4257(94)00061-Q, http://www.sciencedirect.com/science/article/pii/003442579400061Q, remote Sensing of Land Surface for Studies of Global Chage, 1995.

Wang, D., Liang, S., He, T., and Yu, Y.: Direct estimation of land surface albedo from VIIRS data: Algorithm improvement and preliminary validation, Journal of Geophysical Research: Atmospheres, 118, 12,577–12,586, https://doi.org/10.1002/2013JD020417, https://agupubs.onlinelibrary.wiley.com/doi/abs/10.1002/2013JD020417, 2013.

Wendisch, M. and Yang, P.: Theory of atmospheric radiative transfer, John Wiley & Sons, 2012.

Wendisch, M., Müller, D., Schell, D., and Heintzenberg, J.: An Airborne Spectral Albedometer with Active Horizontal Stabilization, Journal of Atmospheric and Oceanic Technology, 18, 1856–1866, https://doi.org/10.1175/1520-0426(2001)018<1856:AASAWA>2.0.CO;2, https://doi.org/10.1175/1520-0426(2001)018<1856:AASAWA>2.0.CO;2, 2001.

Wendisch, M., Macke, A., Ehrlich, A., Lüpkes, C., Mech, M., Chechin, D., Dethloff, K., Barientos, C., Bozem, H., Brückner, M., Clemen, H.-C., Crewell, S., Donth, T., Dupuy, R., Ebell, K., Egerer, U., Engelmann, R., Engler, C., Eppers, O., Gehrmann, M., Gong, X., Gottschalk, M., Gourbeyre, C., Griesche, H., Hartmann, J., Hartmann, M., Heinold, B., Herber, A., Herrmann, H., Heygster, G., Hoor, P., Jafariserajehlou, S., Jäkel, E., Järvinen, E., Jourdan, O., Kästner, U., Kecorius, S., Knudsen, E. M., Köllner, F., Kretzschmar, J., Lelli, L., Leroy, D., Maturilli, M., Mei, L., Mertes, S., Mioche, G., Neuber, R., Nicolaus, M., Nomokonova, T., Notholt, J., Palm, M., van Pinxteren, M., Quaas, J., Richter, P., Ruiz-Donoso, E., Schäfer, M., Schmieder, K., Schnaiter, M., Schneider, J., Schwarzenböck, A., Seifert, P., Shupe, M. D., Siebert, H., Spreen, G., Stapf, J., Stratmann, F., Vogl, T., Welti, A., Wex, H., Wiedensohler, A., Zanatta, M., and Zeppenfeld, S.: The Arctic Cloud Puzzle: Using ACLOUD/PASCAL Multi-Platform Observations to Unravel the Role of Clouds and Aerosol Particles in Arctic Amplification, Bulletin of the American Meteorological Society, 0, https://doi.org/10.1175/BAMS-D-18-0072.1, https://doi.org/10.1175/BAMS-D-18-0072.1, in press.

Winther, J.-G., Bruland, O., Sand, K., Gerland, S., Marechal, D., Ivanov, B., Gøowacki, P., and König, M.: Snow research in Svalbard—an overview, Polar Research, 22, 125–144, https://doi.org/10.3402/polar.v22i2.6451, https://doi.org/10.3402/polar.v22i2.6451, 2003.

Zege, E., Malinka, A., Katsev, I., Prikhach, A., Heygster, G., Istomina, L., Birnbaum, G., and Schwarz, P.: Algorithm to retrieve the melt
pond fraction and the spectral albedo of Arctic summer ice from satellite optical data, Remote Sensing of Environment, 163, 153–164,
https://doi.org/https://doi.org/10.1016/j.rse.2015.03.012, http://www.sciencedirect.com/science/article/pii/S003442571500108X, 2015.

Zhang, Y., Rossow, W. B., Lacis, A. A., Oinas, V., and Mishchenko, M. I.: Calculation of radiative fluxes from the surface to top of at-
5 mosphere based on ISCCP and other global data sets: Refinements of the radiative transfer model and the input data, Journal of Geo-
physical Research: Atmospheres, 109, https://doi.org/10.1029/2003JD004457, https://agupubs.onlinelibrary.wiley.com/doi/abs/10.1029/
2003JD004457, 2004.

Zhang, Y.-C., Rossow, W. B., and Lacis, A. A.: Calculation of surface and top of atmosphere radiative fluxes from physical quantities based
on ISCCP data sets: 1. Method and sensitivity to input data uncertainties, Journal of Geophysical Research: Atmospheres, 100, 1149–1165,
10 https://doi.org/10.1029/94JD02747, https://agupubs.onlinelibrary.wiley.com/doi/abs/10.1029/94JD02747, 1995.

Zhou, Y., Wang, D., Liang, S., Yu, Y., and He, T.: Assessment of the Suomi NPP VIIRS Land Surface Albedo Data Using Station Measure-
ments and High-Resolution Albedo Maps, Remote Sensing, 8, https://doi.org/10.3390/rs8020137, 2016.
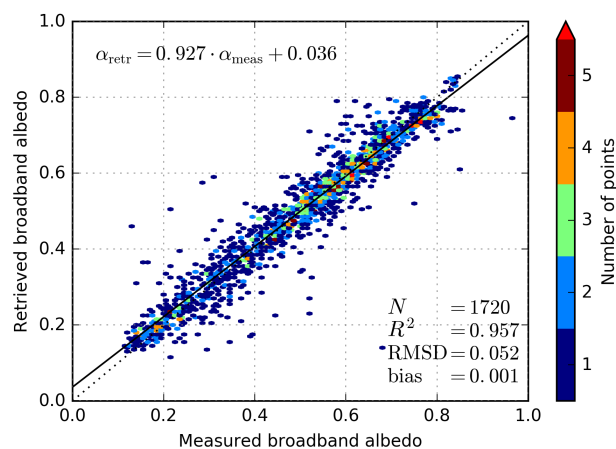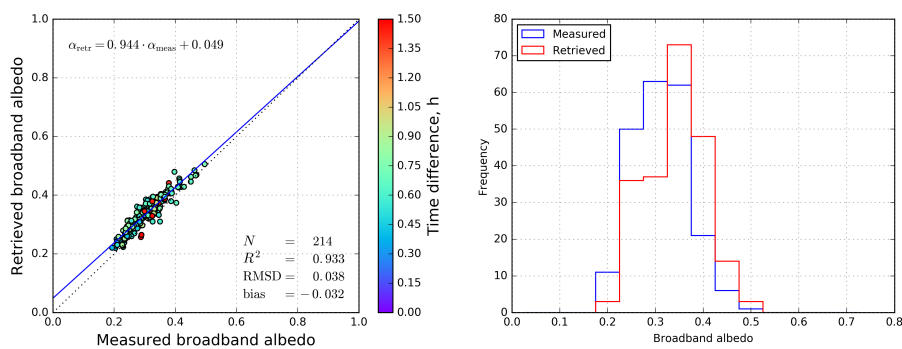
Figure 1. Scatterplot of measured broadband albedo and retrieved broadband albedo by applying the empirically derived STBC to measured spectral albedo. Measurements were done by Polashenski (2011) over landfast ice of different melting stages close to Barrow, AK, USA between April and June of the years 2008 and 2009. Colors indicate the number density of points. The solid and dotted lines indicate the regression and 1-to-1 line, respectively.

The Cryosphere
Discussions

Open Access

EGU
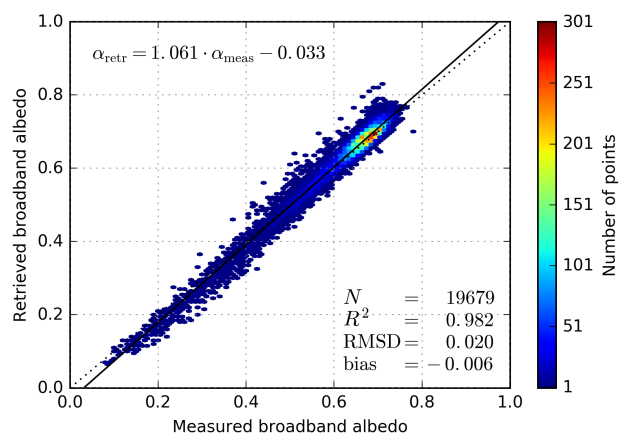
Figure 2. Scatterplot of measured broadband albedo and retrieved broadband albedo by applying the empirically derived STBC to measured spectral albedo. Measurements were done with aircraft Polar 5 over sea ice floes on 25 June 2017. Colors indicate the number density of points. The solid and dotted lines indicate the regression and 1-to-1 line, respectively.
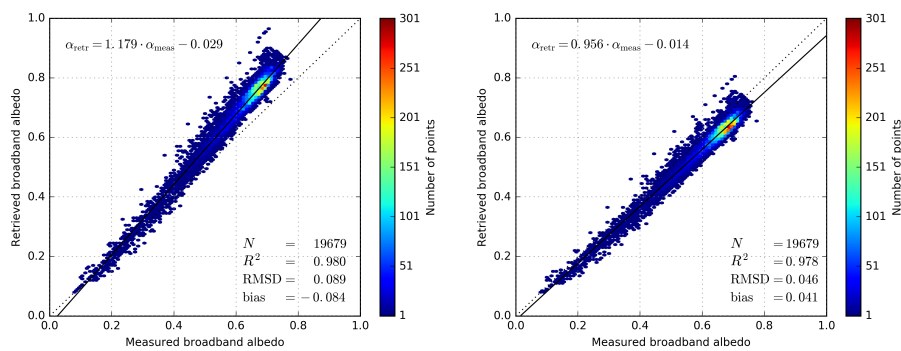
Figure 3. Same as Fig. 2 but using the conversion methods proposed by Istomina et al. (2015) (left) and Gao et al. (2004) (right) instead, respectively.

Figure 4. Scatterplot (left) and histogram (right) of airborne measured and satellite derived broadband albedo on 6 June 2008 over landfast ice (no drift). The color of points define the time difference between airborne measurement and satellite overflight. Regression line and 1-to-1 line are shown in blue solid and black dotted, respectively.
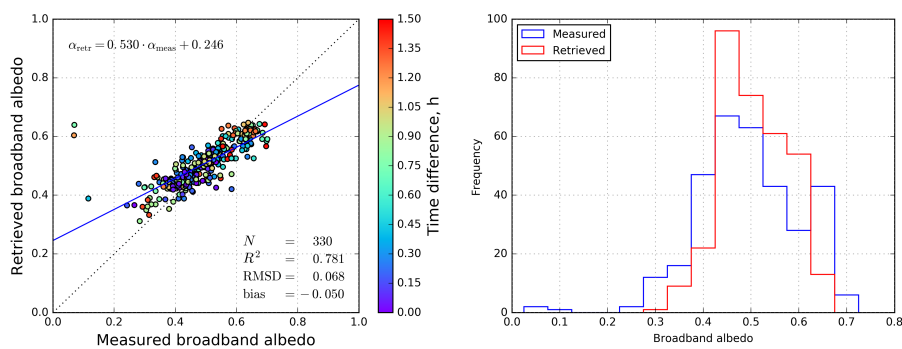
Figure 5. Scatterplot (left) and histogram (right) of airborne measured and satellite derived broadband albedo on 26 May and 3, 4, and 7 June 2008 over sea ice floes (possible sea ice drift contamination). The colors of points define the time difference between airborne measurement and satellite overflight. Regression line and 1-to-1 line are shown in blue solid and black dotted, respectively.
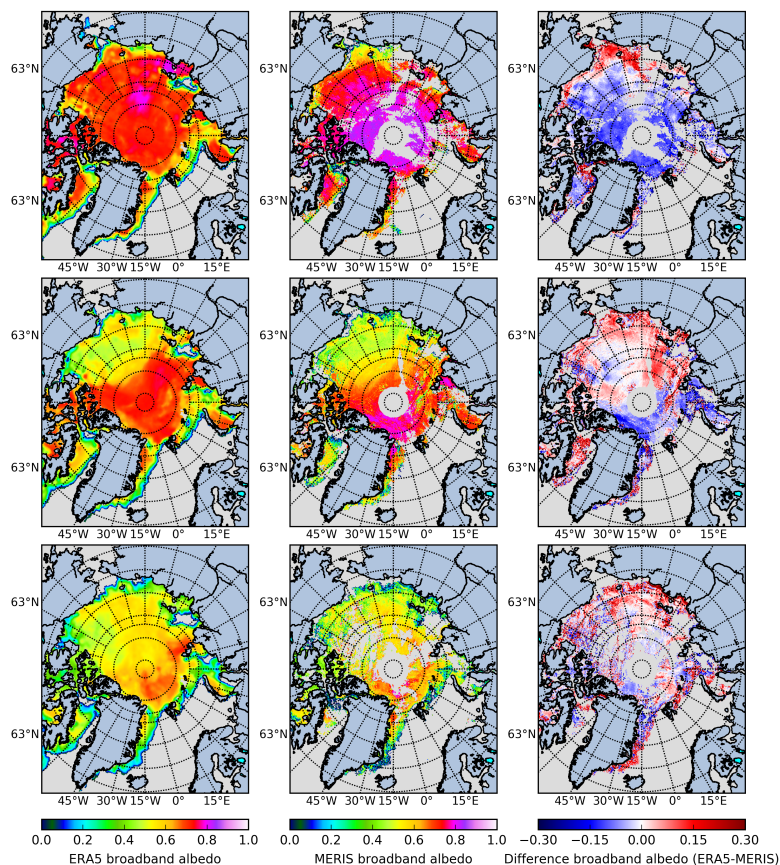
Figure 6. Daily averaged broadband albedo of Arctic sea ice derived from ERA5 irradiances (left) and from MERIS observations (middle) and the difference between both albedo products (right). The data are from 2 (top, before melt onset), 12 (middle, at melt onset), and 25 (bottom, after melt onset) June 2007. Cloud contaminated areas and the satellite pole hole in the MERIS data set are shown in gray. Data are gridded using the NSIDC (National Snow and Ice Data Center) polar stereographic projection.
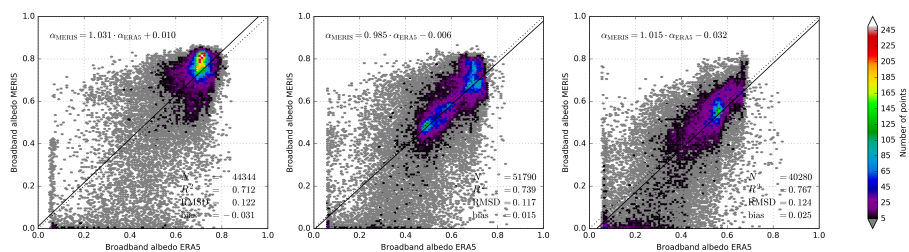
Figure 7. Comparison of ERA5 and MERIS derived broadband albedo of Arctic sea ice on 2 (left, before melt onset), 12 (middle, at melt onset), and 25 (right, after melt onset) June 2007. Regression line and 1-to-1 line are shown in black solid and dotted, respectively.

The Cryosphere
Discussions
Open Access
EGU

Table 1. List of major surface broadband albedo products derived from satellite observations.

Data set name	Instrument	Platform	Spatial resolution	Temporal resolution	Temporal coverage	waveband [μm]	retrieval method	References
-	MODIS	Terra, Aqua	1 km / 0.05 °	8 days	2000 – now	0.3 - 5	kernel driven BRDF, NTBC	Lucht et al. (2000), Schaaf et al. (2002)
APP-x	AVHRR	NOAA POES	5 km	Twice daily (Arctic region)	1982 – now	0.28 - 4	NTBC, ARC	Key et al. (2016)
-	VIIRS	S-NPP	1 km	1 day / 16 days	2011 – now	0.4 - 4	Direct estimation	Wang et al. (2013), Zhou et al. (2016)
-	OLI	Landsat	30 m	16 days	2013 – now	0.3 - 3	Direct estimation	He et al. (2018a, b)
-	TM/ETM+	Landsat	30 m	16 days	1982 – now	0.3 - 3	Direct estimation	He et al. (2018a, b)
-	MERIS	ENVISAT	1 km / 0.05 °	1 day	2002–2012	0.4 - 0.9	Analytic solution of RTT, STBC	Zege et al. (2015), Istomina et al. (2015)
Glob-Albedo	VEGETATION, AATSR, MERIS, MODIS	SPOT, ENVISAT, Terra, Aqua	1 km / 0.05 °, 0.5 °	16 days / 1 month	1998-2011	0.3 - 3	NTBC, kernel driven BRDF	Muller et al. (2012), Lewis et al. (2013)
GLASS	MODIS, AVHRR	Terra, Aqua, NOAA	1 km / 0.05 °	1 day / 8 days	1981-2012	0.3 - 3	Direct estimation	Liu et al. (2013), Liang et al. (2013)
CERES-EBAF	CERES	Terra, Aqua, S-NPP, NOAA	1 °	1 day / 1 month	2000 - now	0.3 - 5	RTT	CERES-EBAF (2014), Loeb et al. (2018)
ISCCP	VISSR, MIR, AVHRR	GMS, GOES, INSAT, METEOSAT, NOAA	2.5 °	1 month	1983-2009	0.2 - 5	RTT	Zhang et al. (1995, 2004), Schiffer and Rossow (1983)

Table 2. Coefficients k_i from Eq. (1) to calculate MERIS broadband albedo from spectral albedo at the six wavelengths $400, 500, 600, 700, 800,$ and 900 nm (for Gao et al. (2004) from the narrowband albedo at channels with the center wavelengths $490, 560, 665,$ and 865 nm).

	k_0	k_1	k_2	k_3	k_4	k_5	k_6
Empirically derived	0.0000	0.9337	-2.0856	2.9125	-1.6231	0.6750	0.0892
Istomina et al. (2015)	0.0000	0.1666	0.1666	0.1666	0.1666	0.1666	0.1666
Gao et al. (2004)	0.0149	0.1587	-0.2463	0.5442	0.3748	0.0000	0.0000

Table 3. Times of airborne measurements (Polar 5) and satellite overflights (MERIS on ENVISAT) in UTC for selected days during the MELTEX campaign in 2008.

	26 May 2008	3 June 2008	4 June 2008	6 June 2008	7 June 2008
Polar 5	20:45-21:48	17:00-19:46	19:14-23:24	19:01-21:55	17:08-20:17
MERIS	20:46	19:54	21:02	20:00	21:08